SUPPLEMENTAL DATA

A 'Molecular Brake' in the Kinase Hinge Region Regulates the Activity of Receptor Tyrosine Kinases

Huaibin Chen, Jinghong Ma, Wanqing Li, Anna V. Eliseenkova, Chongfeng Xu, Thomas A. Neubert, W. Todd Miller, and Moosa Mohammadi

Figure Legends

Figure S1. Sequence alignment of the intracellular domains of human FGFR1 to 4 based on the crystal structures of unphosphorylated and A-loop tyrosine phosphorylated wild-type FGFR2K. Secondary structures were assigned using PROCHECK (Laskowski et al., 1993), and are shown above the sequence alignment. Blue and red bars denote strands and helices, respectively. For comparison, the secondary structure assignments for the unphosphorylated wild-type structure appear on top of those for A-loop tyrosine phosphorylated wild-type structure. The location of the residues at which pathogenic mutations in FGFR2 and FGFR3 occurs are colored green. The A-loop twin tyrosine phosphorylation sites are colored orange. The sequences and secondary structures of phosphorylated IRK and IGF1RK are also shown. The A-loop, kinase hinge and kinase insert are highlighted with green, yellow and black boxes, respectively.

Figure S2. **(A)** Stereo view of the Cα traces of unphosphorylated (in orange) and A-loop tyrosine phosphorylated (in green) wild-type FGFR2K structures following the superimposition of the C-lobes. The diverging and converging points of the A-loops are denoted by arrow heads. **(B)** The αC helix in FGFR2 kinase does not shift independently of the other secondary structure elements of the N-lobe upon activation. unphosphorylated (in gray) and A-loop tyrosine phosphorylated (in green) wild-type FGFR2K structures following superimposition of the N-lobes are shown in cartoon (in two views). **(C)** The salt bridge between K517 in the β3 strand and E534 in the αC helix is already taking place in the unphosphorylated wild-type FGFR2K structure.

Figure S3. All FGFR2K pathogenic mutations disengage the molecular brake at the kinase hinge region and cause an inward rotation of the N-lobe towards the C-lobe. **(A)** Comparison of the disposition of the kinase N-lobes in wild-type (either unphosphorylated and A-loop tyrosine phosphorylated) and different unphosphorylated mutant FGFR2K structures following superimposition of the C-lobes (not shown for clarity). The pivot point, located between I548 and N549, is indicated by an arrow. To better illustrate the N-lobe rotation, a close-up view of the N-terminal segment of the αC helix is shown in the inset. **(B)** Representation of the hydrogen bonding between D530 in the αC helix and R664 in the A-loop, as exemplified by the E565G mutant FGFR2K structure (in green). Note that this hydrogen bonding does not occur in the unphosphorylated wild-type FGFR2K structure (in wheat).

Figure S4. Positive (**(A)** to **(D)**) and negative ion (**(E)**) MALDI Q-TOF mass spectra of methyl-esterified tryptic digests of FGFR2K wild-type and mutant kinases. **(A)** N549H mutant FGFR2K; **(B)** R678G mutant FGFR2K; **(C)** unphosphorylated wild-type FGFR2K; **(D)** and **(E)** A-loop phosphorylated wild-type FGFR2K. The A-loop peptide, DINNIDYYKK (theoretical monoisotopic MW=1284.64 before methyl esterification and 1326.68 after methyl esterification), with 0 to 2 tyrosine phosphorylations, are labeled with (#), (*), (**) respectively. Methyl ester side products of deamidated Asn (N) residues are labeled (+15). Methyl esterification was performed to increase the selectivity for the detection of phosphopeptides (Xu et al., 2005). **(F)** shows the MS spectrum of the A-loop peptide with 1 or 2 tyrosine phosphorylations (calculated MH^+1365.61 and 1385.58, respectively) from a tryptic digest of dissolved crystal after enrichment for phosphopeptides using TiO_2 chromatography. **(G)** shows the MS/MS spectrum of the monophosphorylated peptide at MH^+1365.61.

Figure S5. Stereo view of the molecular brake at the kinase hinge region of unphosphorylated and phosphorylated wild-type and 7 unphosphorylated mutant FGFR2Ks with the $2F_O$-F_C electron density map contoured at 1σ around the hinge region. Coloring scheme is as in **Fig. 3**.

Figure S6. Evaluation of the conformational changes between the unphosphorylated wild-type FGFR2K structure and the phosphorylated wild-type and 7 unphosphorylated mutant FGFR2K structures using difference distance matrix plot (DDMP) program. The two regions with greatest conformational changes are denoted by red and cyan bars.

Table S1. Kinetic properties of wild-type and mutant FGFR2Ks

1. Variable substrate = RTK peptide (KKEEEEYMMMMG)

Protein	**$K_{m,\ peptide}$ (μM)**	**V_{max} (nmol/min/mg)**	**k_{cat}/K_m (min^{-1} mM^{-1})**
WT	450 ± 60	350 ± 16	28
K659N	980 ± 100	4140 ± 170	157
E565A	1030 ± 100	16450 ± 840	595

2. Variable substrate = STAT1 peptide (GPKGTGYIKTELISVSG)

Protein	**$K_{m,\ peptide}$ (μM)**	**V_{max} (nmol/min/mg)**	**k_{cat}/K_m (min^{-1} mM^{-1})**
WT	620 ± 180	450 ± 60	27
K659N	460 ± 160	10230 ± 1220	828
E565A	430 ± 170	7930 ± 140	686

3. Variable substrate = ATP

Protein	**$K_{m,\ ATP}$ (μM)**	**V_{max} (nmol/min/mg)**	**k_{cat}/K_m (min^{-1} mM^{-1})**
WT	840 ± 140	480 ± 30	21
K659N	1540 ± 110	4920 ± 320	119
E565A	300 ± 60	4580 ± 300	571

Table S2. Data Collection and Refinement Statistics

Construct	Unphos. WT	Phos. WT	N549H	N549T	E565G
Data Collection					
Resolution (Å)	50-2.4 (2.49-2.4)	50-1.8 (1.86-1.8)	50-2.4 (2.49-2.4)	50-2.4 (2.49-2.4)	50-2.3 (2.38-2.3)
Space group	$P2_12_12$	$P2_12_12_1$	$P2_12_12$	$P2_12_12$	$P2_12_12$
Unit Cell Parameters (Å, °)	a=106.610 b=118.605 c=63.124	a=56.353 b=78.436 c=84.839	a=105.521 b=117.50 c=63.174	a=105.043 b=114.474 c=64.347	a=104.897 b=114.748 c=64.440
Content of the asymmetric unit	2	1	2	2	2
Measured reflections (#)	221513	182181	303612	185633	187739
Unique Reflections (#)	31998 (3117)	35199 (3478)	30784 (2993)	29605 (2631)	34867 (3243)
Data redundancy	6.9 (5.8)	5.2 (5.1)	9.9 (8.8)	6.3 (5.6)	5.4 (3.8)
Data completeness (%)	99.6 (98.4)	98.6 (98.6)	99.3 (98.3)	95.0 (86.1)	99.1 (93.8)
R_{sym} (%)	10.2 (34.8)	4.6 (26.7)	6.5 (23.3)	7.2 (25.6)	6.4 (22.6)
I/sig	12.7	30.9	15.2	18.5	20.3
Refinement					
R factor/R free	21.1/25.8	25.1/26.5	20.1/23.8	21.4/25.4	21.7/25.2
Number of protein atoms	4517	2318	4465	4440	4440
Number of non-protein/solvent atoms	20	33	74	86	86
Number of solvent atoms	188	119	133	160	172
Rmsd bond length (Å)	0.006	0.006	0.006	0.00	0.006
Rmsd bond angle (°)	1.2	1.3	1.3	1.3	1.3
Rmsd B factor ($Å^2$)	2.1	1.2	1.2	1.9	1.1
PDB ID	2PSQ	2PVF	2PWL	2PZ5	2PY3

[a] Numbers in parenthesis refer to the highest resolution shell.

[b] $Rsym = \sum|I - \langle I \rangle| / \sum I$, where I is the observed intensity of a reflection, and $\langle I \rangle$ is the average intensity of all the symmetry related reflections.

Table S2. Data Collection and Refinement Statistics (cont.)

Construct	E565A	K641R	K526E	K659N
Data Collection				
Resolution (Å)	50-2.9 (3.0-2.9)	50-3.0 (3.11-3.0)	50-2.4 (2.49-2.4)	50-2.2 (2.28-2.2)
Space group	$P2_12_12$	$P2_12_12$	$P2_12_12$	P1
Unit Cell Parameters (Å, °)	a=105.569 b=116.824 c=63.942	a=106.137 b=116.642 c=63.636	a=105.410 b=114.021 c=64.392	a=70.581 b=70.467 c=85.690 α=92.185 β=112.305 γ=116.187
Content of the asymmetric unit	2	2	2	4
Measured reflections (#)	116167	115823	187454	155806
Unique Reflections (#)	17986 (1699)	16398 (1606)	29906 (2796)	65751 (6369)
Data redundancy	6.5 (5.7)	7.1 (7.2)	6.3 (5.6)	2.4 (1.9)
Data completeness (%)	99.4 (97.4)	100 (100)	96.5 (92.2)	97.7 (95.3)
R_{sym} (%)	15.9 (50.6)	11.7 (31.4)	7.1 (25.2)	4.0 (13.1)
I/sig	8.2	11.4	17.8	30.3
Refinement				
R factor/R free	20.2/25.2	20.1/26.8	21.4/25.1	24.4/28.1
Number of protein atoms	4415	4417	4434	8919
Number of non-protein/solvent atoms	40	40	86	88
Number of solvent atoms	60	49	147	163
Rmsd bond length (Å)	0.007	0.007	0.006	0.008
Rmsd bond angle (°)	1.3	1.3	1.3	1.3
Rmsd B factor ($Å^2$)	2.2	2.2	1.8	1.1
PDB ID	2Q08	2PZR	2PZP	2PVY

[a] Numbers in parenthesis refer to the highest resolution shell.

[b] $Rsym = \sum|I - < I >|/\sum I$, where I is the observed intensity of a reflection, and $< I >$ is the average intensity of all the symmetry related reflections.

Table S3. N-lobe rotation and the A-loop conformation of wild-type and mutant FGFR2Ks

	Unphos.WT	Phos. WT	N549H	N549T	E565G	E565A	K641R	K526E	K659N
N-lobe rotation*	-	6.7°	4.2°	7.0°	6.8°	5.7°	5.2°	6.5°	5.6
A-loop conformation	Inactive	Active	Inactive	Inactive	Inactive	Inactive	Inactive	Inactive	Active

*The degrees of N-lobe rotation were calculated using program lsqkab from CCP4 suite. First, the C-lobe of phosphorylated wild-type or different mutant FGFR2 kinases were superimposed onto that of unphosphorylated wild-type FGFR2 kinase (reference structure). Thereafter, the N-lobes of transformed phosphorylated wild-type or the transformed mutant FGFR2K structures were superimposed onto that of unphosphorylated wild-type FGFR2K structure.

F) Supplemental Figure 1

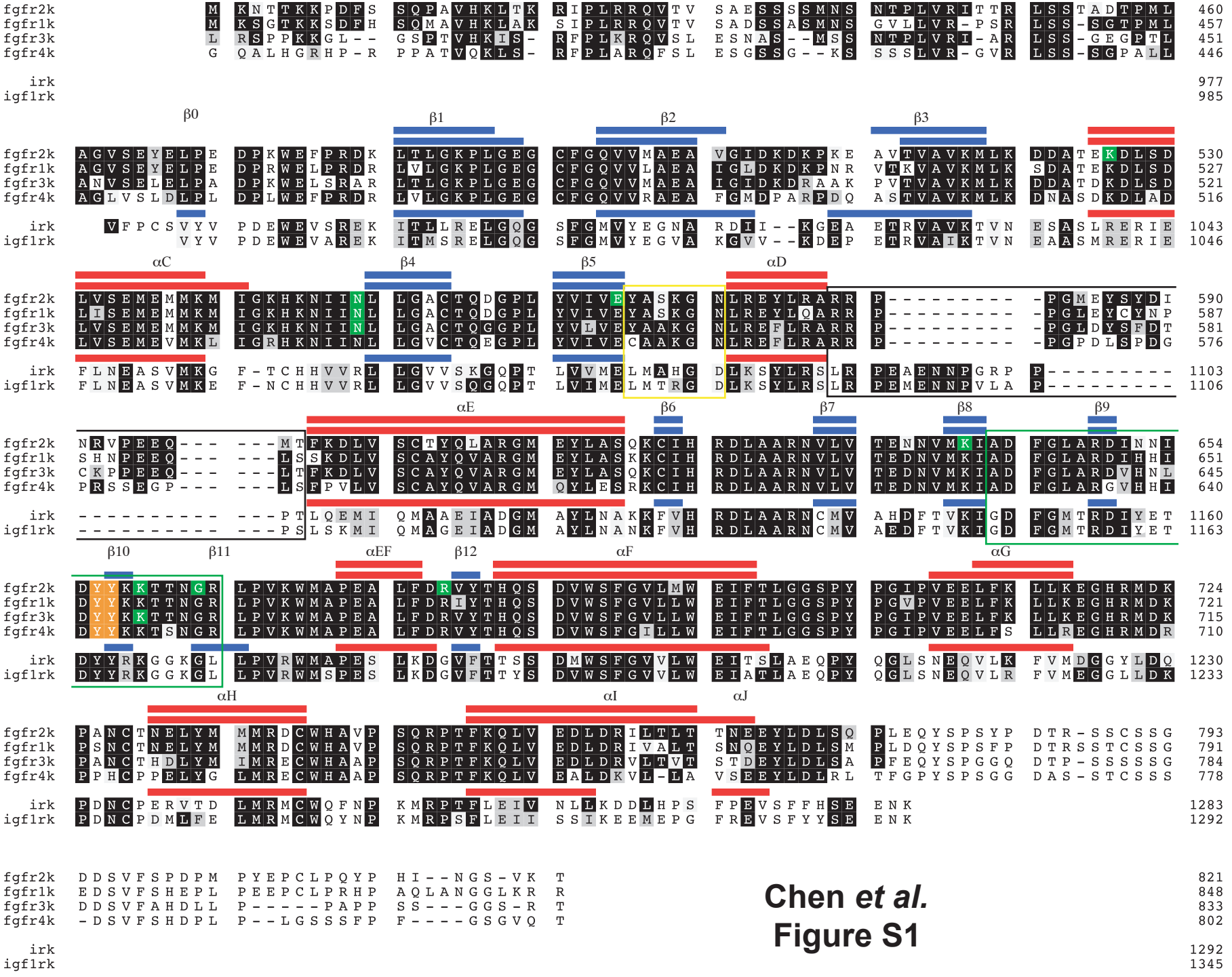

Chen *et al.*
Figure S1

F) Supplemental Figure 2

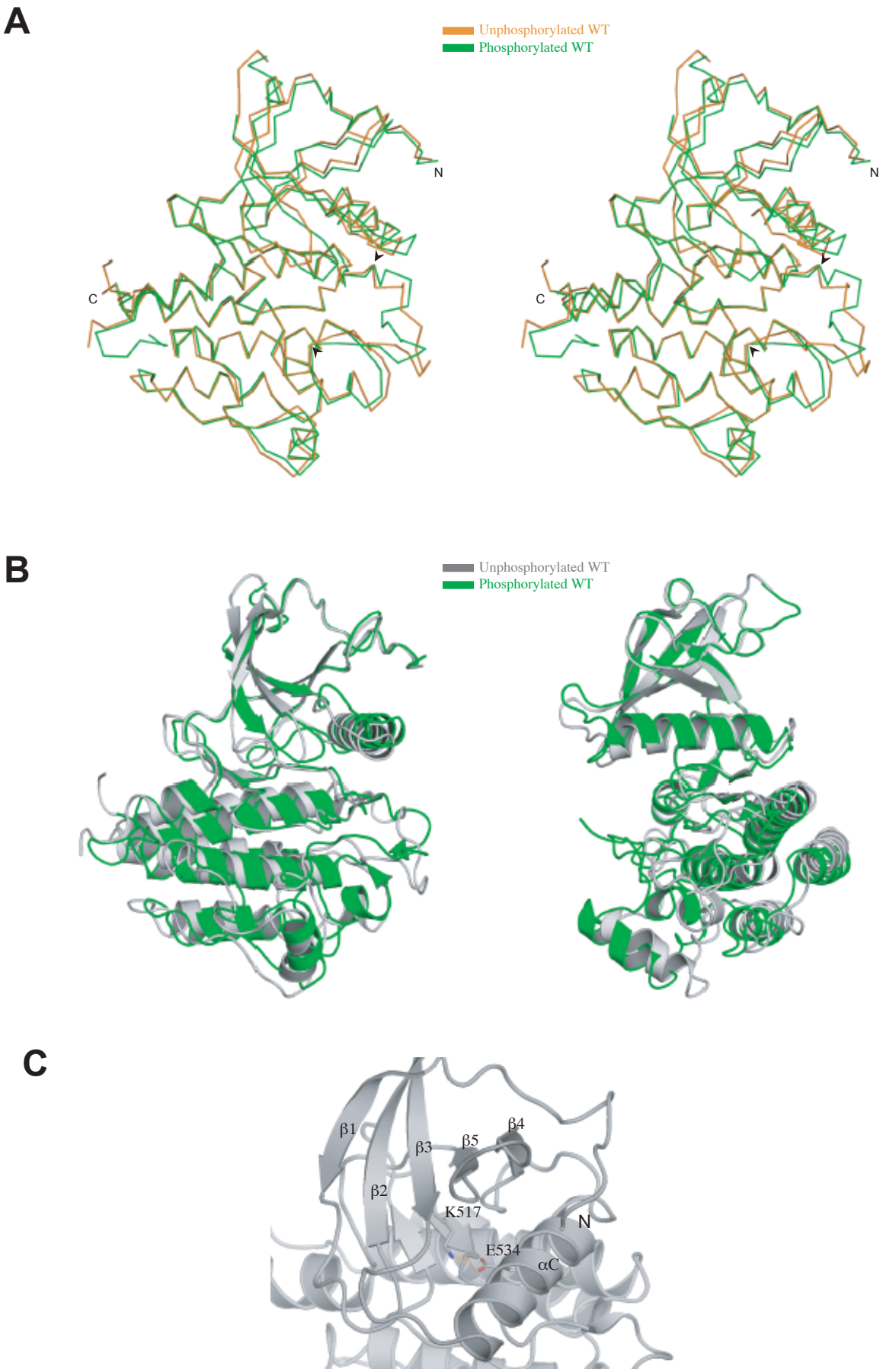

Chen *et al.*
Figure S2

F) Supplemental Figure 3

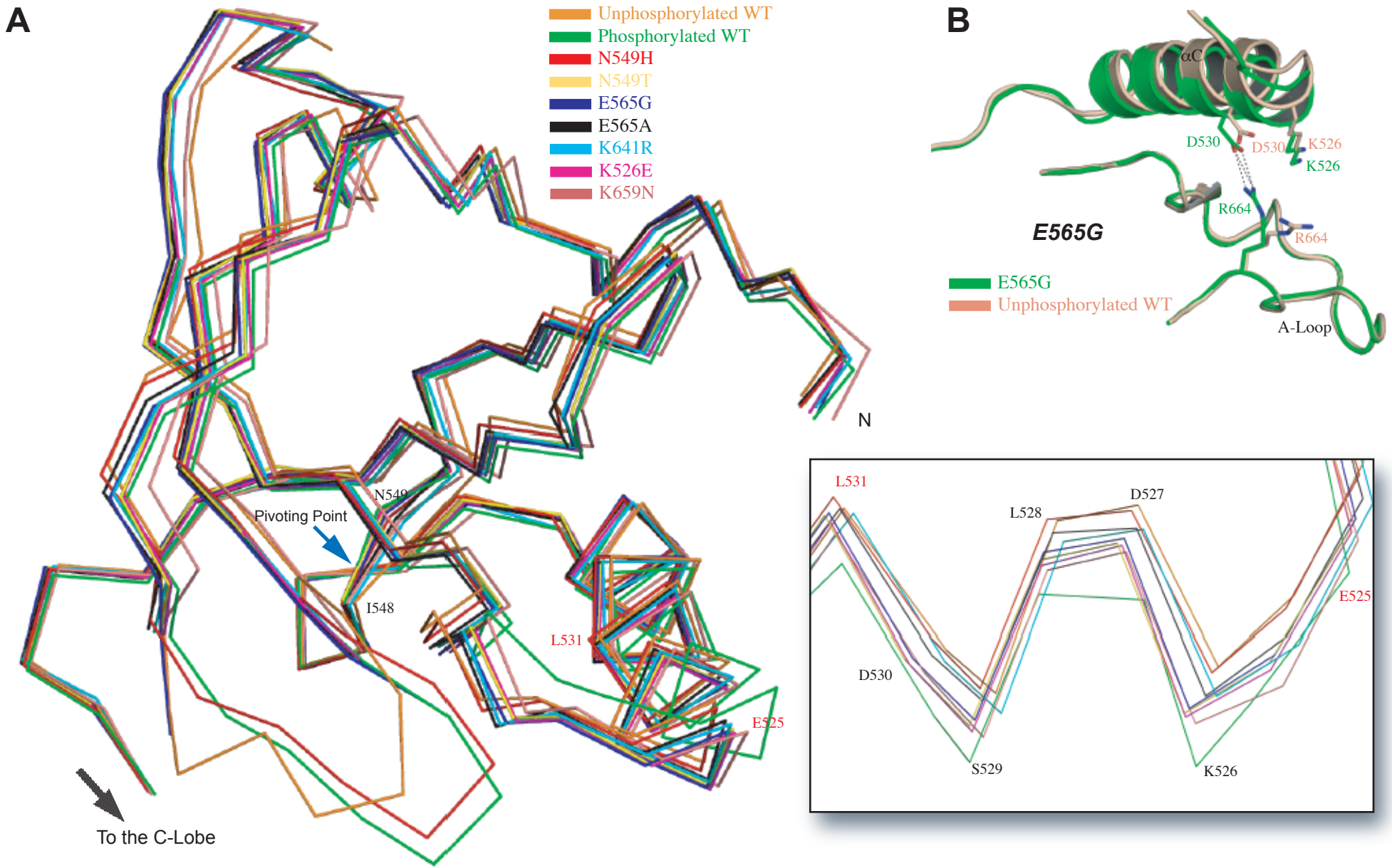

Chen *et al.*
Figure S3

F) Supplemental Figure 4

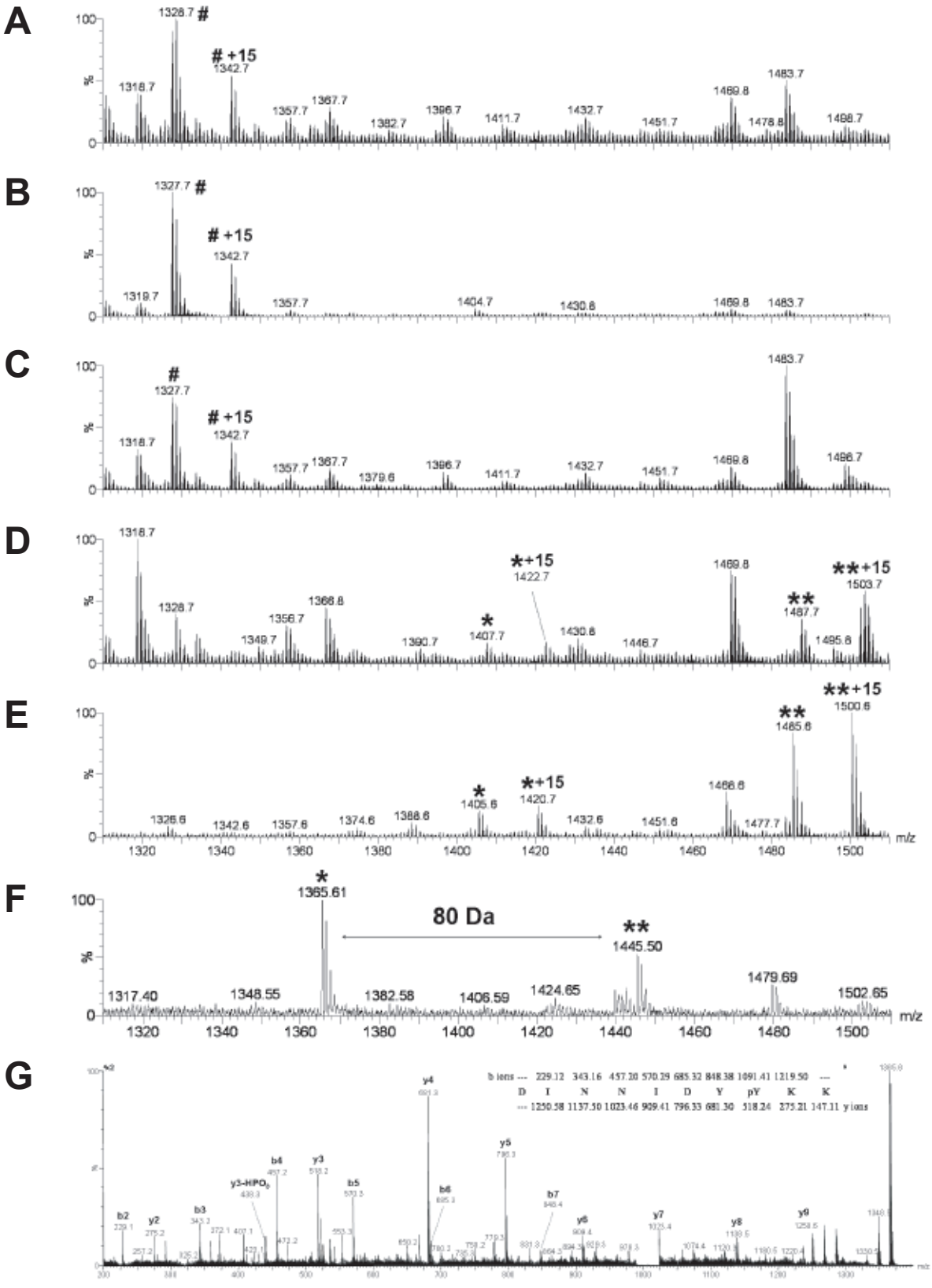

Chen *et al.*
Figure S4

F) Supplemental Figure 5

Unphos. WT

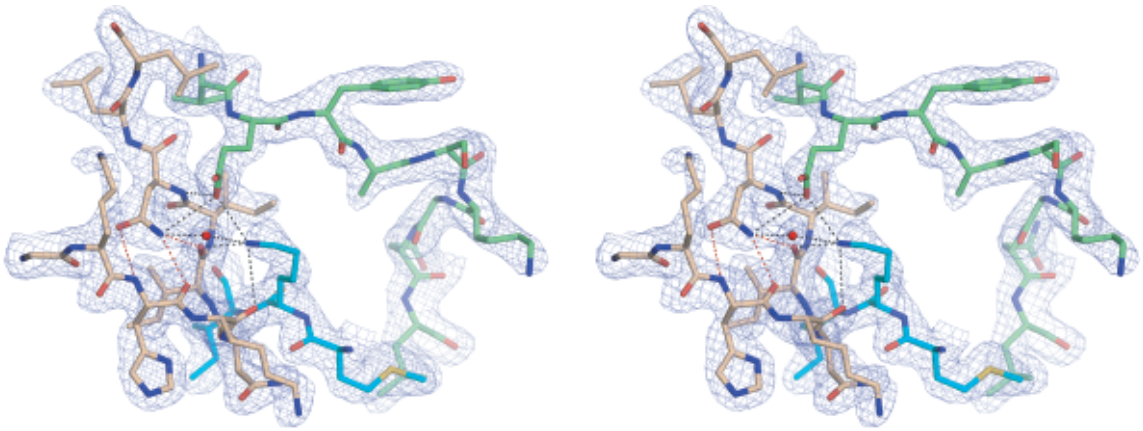

Phos. WT

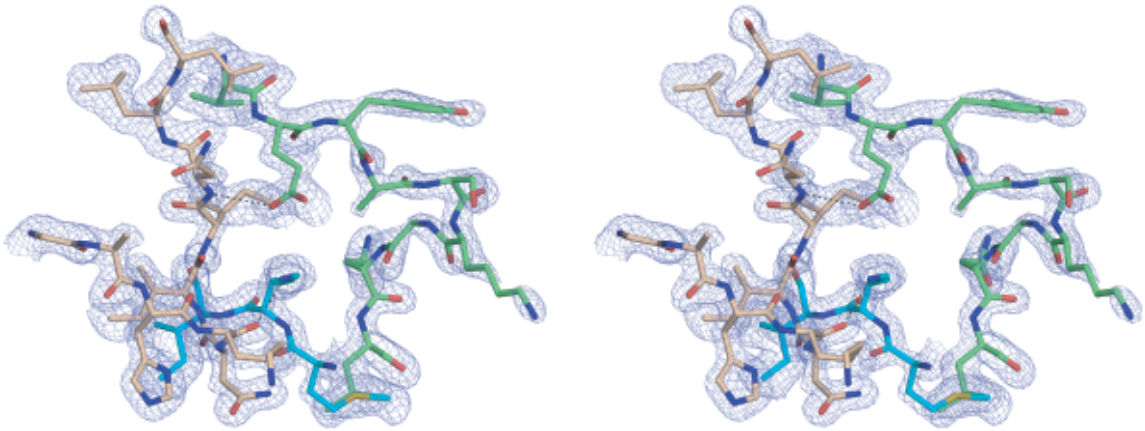

N549H Mutant

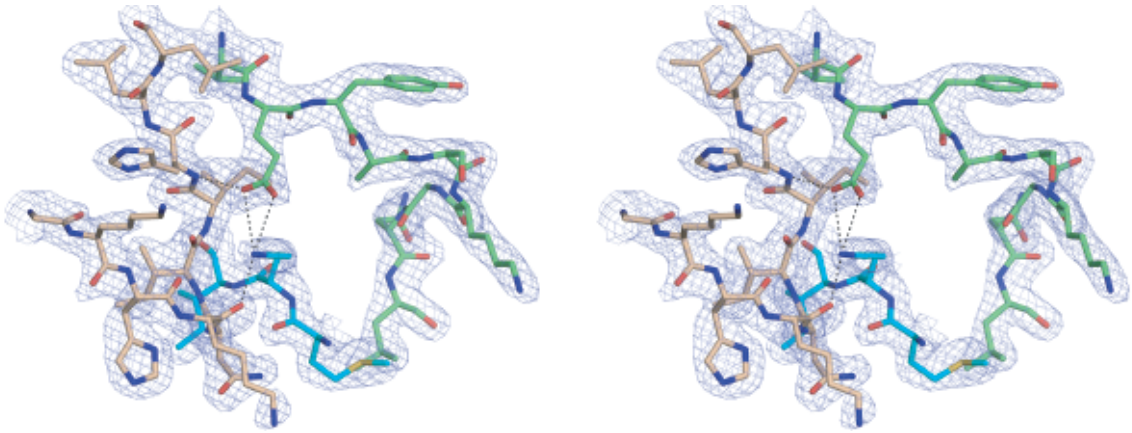

N549T Mutant

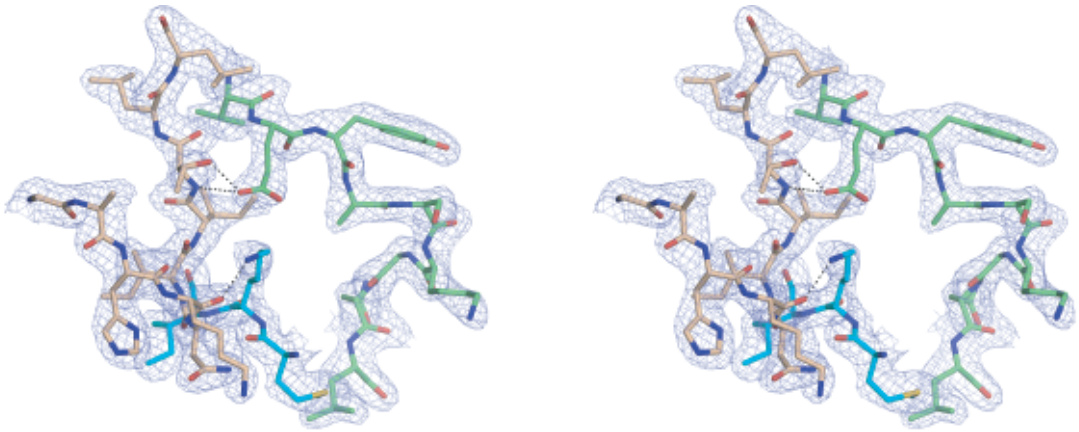

Chen *et al.*
Figure S5

E565G Mutant

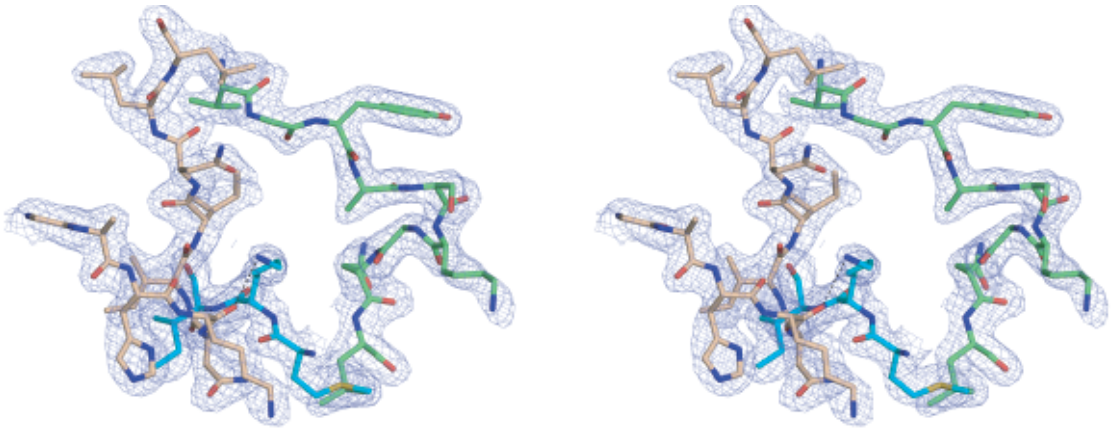

E565A Mutant

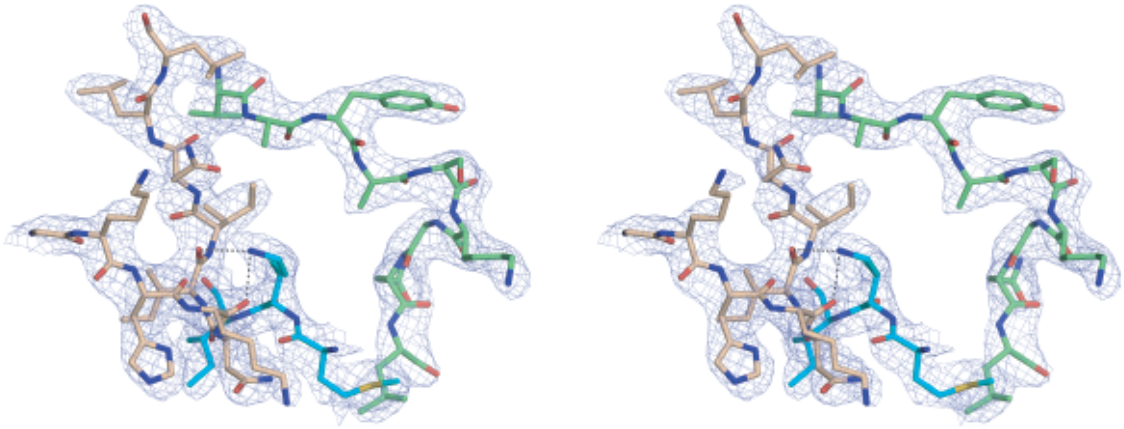

K641R Mutant

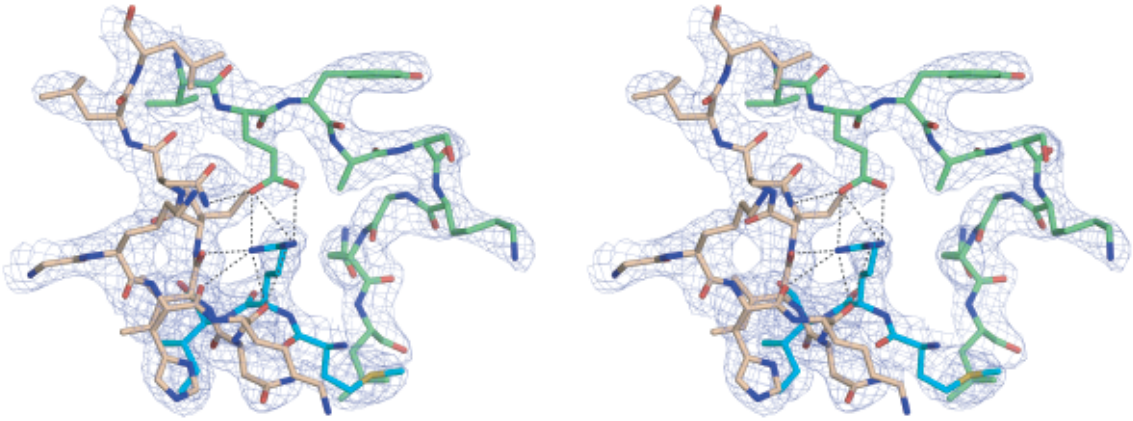

K526E Mutant

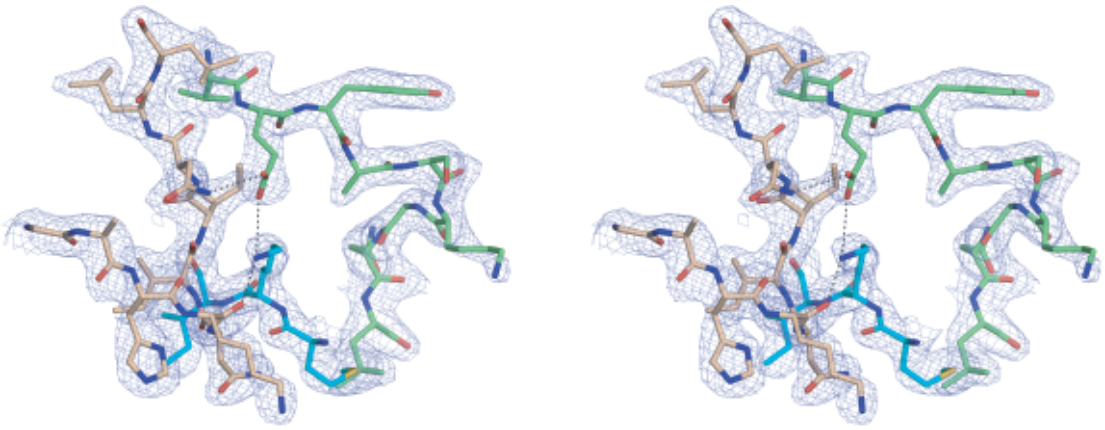

Chen *et al.*
Figure S5 (cont.)

K659N Mutant

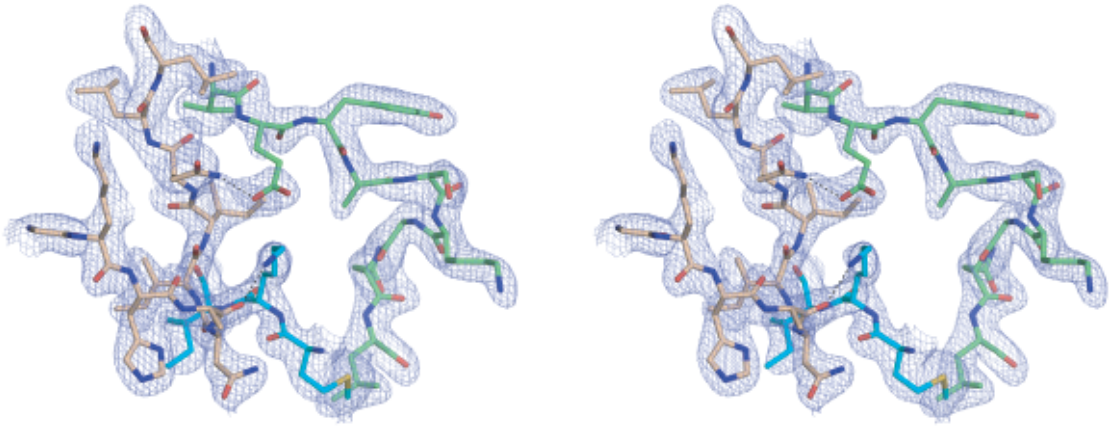

Chen *et al.*
Figure S5 (cont.)

F) Supplemental Figure 6

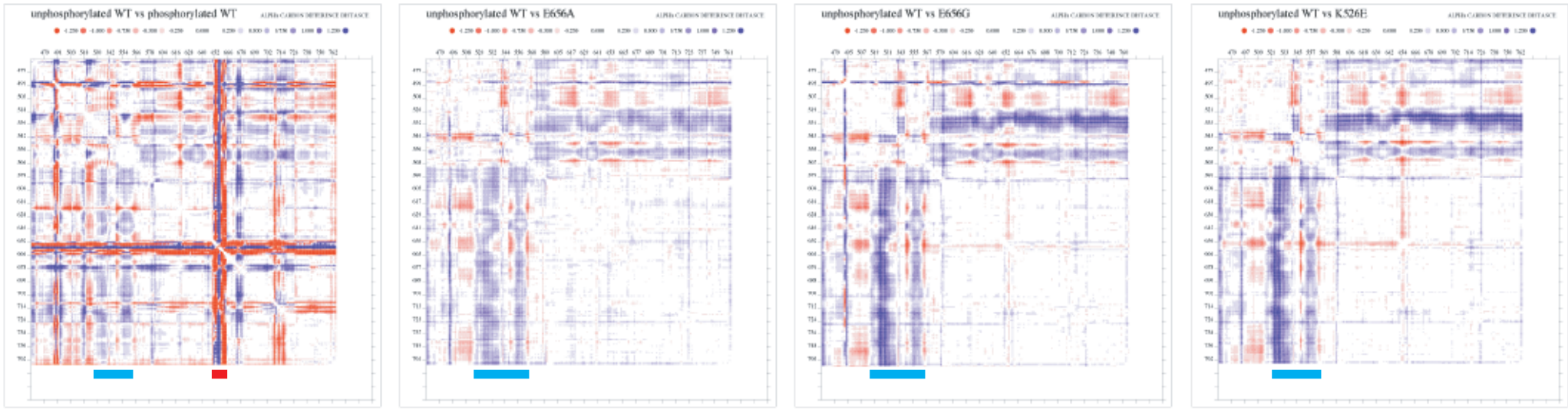

Residue 652 to 664 of the A-loop

Residue 520 to 568 consisting of the β3-αC loop, αC helix, αC-β4 loop, β4 strand, β4-β5 loop, β5 strand and the first three residues of the kinase hinge

Chen *et al.*
Figure S6